Int. J. Adv. Eng. Pure Sci. 2023, 35(1): 18-26
DOI: 10.7240/jeps.1141264

RESEARCH ARTICLE / ARAŞTIRMA MAKALESİ

The Effect of Pressure on Anisotropic Elastic Properties of SbSeI: DFT Calculation

Tahsin Özer 1

[1] *Osmaniye Korkut Ata University Bahce Vocational High School, Osmaniye, Turkiye.*

Abstract

The mechanical and elastic properties of SbSeI compound under hydrostatic pressure of 0-40 kBar were investigated for the first time. Quantum Espresso software (QE) was used for all calculations. Elastic constants (C_{ij}) were calculated using the ElaStic package distributed with the QE software and using the energy calculation method in this package. According to the elastic constants obtained, the SbSeI compound was found to be mechanically stable. The results obtained at ambient pressure were found to be in perfect agreement with the literature data. Mechanical properties (bulk modulus, shear modulus, Young's modulus, and Poisson's ratio), anisotropy, linear compressibility, Debye temperatures, Vickers hardness, and minimum thermal conductivity of the SbSeI compound were calculated using these constants. As a result of the calculations, it was seen that the SbSeI compound is a soft (Vickers hardness < 10 *GPa*) and anisotropic material.

Keyword: SbSeI, Pressure effect, Mechanical properties, Quantum Espresso.

1. INTRODUCTION

Bulk V-VI-VII semiconductors are reported to be abundant on earth [1]. The Antimony selenoiodide (SbSeI) compound is a member of the family of semiconductor solids of the V-VI-VII type. Here V-VI-VII shows the group numbers on the periodic table. It symbolizes the atoms V (As, Sb, Bi), VI (S, Se, Te) and VII (Cl, Br, I). SbSeI, which is a Chalcogen, has a stoichiometry of 1: 1: 1 and crystallizes in a crystal structure known as the SbSI type [2]. Triple chalcohalide materials based on the group V-VI-VII elements form a class with useful and interesting properties that exhibit a wide application potential [3]. It has a wide range of application such as microelectronics, optoelectronics, thermoelectric. These facts caused intense investigation.

SbSeI belongs to the chalcohalide materials group. SbSeI is produced from mixtures of the elements antimony (Sb), selenium (Se) and iodine (I) or from mixtures of Sb_2Se_3 and SbI_3 [3]. SbSeI is a semiconductor material, it has pyroelectric, thermoelectric, ferroelectric, piezoelectric, electromechanical, and electrocaloric properties. It is also an excellent candidate for SbSeI photovoltic devices and radiation detectors [4]. These compounds are influenced by light causing other nonlinear optical effects such as photoferroelectrics, pyro-optic, and electro-optical [5] and a good photoconductor [6]. A few chalcohalides such as SbSI and SbSeI were considered promising photoferroic materials due to their favorable band gap and ferroelectric properties [7].

It has been reported that the lattice parameters of SbSeI are a = 8.698 (2) *Å*, b = 4.127 (1) *Å*, c = 10.412 (2) *Å* [8]. SbSeI crystal has two phases as antiferroelectric (T < 410 *K*) and paraelectric phase (PE) (T> 410 *K*) [9], all atoms are in the 4c Wyckoff position [10]. Structure of SbSeI compound at ambient pressure [8], [11] electronic structure [12]–[14] linear optical and electronic structure [15], mechanical, dynamic, thermodynamic properties [2], [16], [17] and electrical conductivity [3] were investigated. As potential optoelectronic materials, Ran et al. (2018) studied antimony-based oxyhalides and chalcohalides [18].

Theory and calculations have played a crucial role in improving our understanding of material properties and have provided guidelines for searching and designing new materials [19]. Chalcohalide alloys have been an important research topic due to their wide variety of properties. As materials mature and commercial applications come closer, the mechanical properties of materials become an important factor for both their processing and end use [20]. Due to this importance, the subject of investigating the mechanical properties of SbSeI was preferred.

2. MATERIAL METHOD

First principal calculations were performed to reveal the mechanical properties of SbSeI under pressure up to 40 *kBar*. The calculations were carried out by adopting ab initio density functional theory (*DFT*) [21], [22] within the Quantum Espresso (QE) software package [23]. Total energy calculations were done with QE software. $5s^2$ p^3 for Sb atom, $4s^2$ p^3 for Se atom and $5s^2$ p^5 electrons for I atom were taken as real

Corresponding Author: TAHSİN ÖZER, Tel: 0328 827 10 00-dahili 5221, e-posta: tahsinozer@osmaniye.edu.tr

Submitted: 06.07.2022, **Revised:** 25.12.2022, **Accepted:** 08.01.2023

valence electrons. In this study, PAW type pseudopotential files and Local Density Approximation (*LDA*) were preferred. The electronic wave functions were enlarged in plane wave basis to initiate a kinetic energy cut off (E_{cut}) 130 Ry, and electronic charge density (E_{cutrho}) was taken as 520 Ry. For k-space summation the 4x4x10 Monkhorst and Pack [24] gamma centered grid of k-points have been used for SbSeI. Optimized values of E_{cut}, E_{cutrho}, k-point were used in all operations. The input files used in the energy calculation were produced with the ElaStic software using the energy calculation method and the results were analyzed with this software [25].

3. FINDINGS AND DISCUSSION

As the first step in the calculations, structural optimization of SbSeI compound at ambient pressure (zero pressure) was performed. The molecular structure of SbSeI compound was visualized with VESTA software [26] using the data obtained as a result of structural optimization for ambient conditions (Figure 1). As shown in Figure 1, the unit cell of the SbSeI compound contains four molecules and 12 atoms and is in the space group *Pnma*- D_{2h}^{16} (no: 62) in orthorhombic structure. Using these values, 4, 8, 12, 16 and 40 kBar hydrostatic pressure was applied to the system. The analyzes showed that the structure did not undergo a phase transition at the pressures studied. Geometric optimization was made for each pressure value. The results obtained were used in elastic constant calculations.

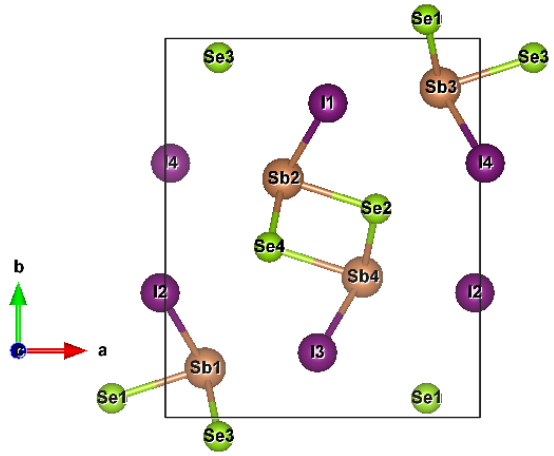

Figure 1. Crystal structure of SbSeI compound.

3.1 The Elastic Constants

Elastic constants can be calculated for many properties of material such as the mechanical stability, anisotropic behavior, ductility, brittleness, specific heat, thermal expansion, Debye temperature and Gruneisen parameters [27]. These properties are very important in design of material. For example, it is desirable that the material designed as piercing and cutting tool is hard.

For an orthorhombic system, there are nine independent elastic constants exist: C_{11}, C_{22}, C_{33}, C_{44}, C_{55}, C_{66}, C_{12}, C_{13} , and C_{23} which are presented in Table 1. As shown in Table 1, the values obtained in this work are consistent with the literature data given for 0 *kBar*.

Table 1. Elastic constants of SbSeI compound calculated at different hydrostatic pressure (*P* in *kBar*, C_{ij} in *GPa*).

P		C_{11}	C_{22}	C_{33}	C_{44}	C_{55}	C_{66}	C_{12}	C_{13}	C_{23}
0	*	38.20	61.10	34.70	8.30	21.00	10.70	16.30	17.20	20.50
0	**	39.23	62.45	33.53	9.11	21.26	10.73	16.03	16.59	19.44
4	*	43.30	63.50	39.10	10.30	23.00	11.70	18.20	19.20	21.70
8	*	48.40	66.90	43.90	12.00	25.90	13.60	21.00	20.40	24.80
12	*	53.40	69.80	50.60	14.00	28.80	14.90	21.70	22.40	27.00
16	*	57.90	72.50	55.50	16.60	31.40	16.30	23.60	23.80	29.20
40	*	82.70	87.60	81.20	26.90	44.10	24.30	35.00	30.20	41.00

* This work, ** [16]

Conventional mechanical stability conditions on elastic constants in orthorhombic systems [28],

$$\begin{aligned} &(C_{22}+C_{33}-2C_{23})>0, \\ &(C_{11}+C_{22}+C_{33}+2C_{12}+2C_{13}+2C_{23})>0 \\ &(C_{11}+C_{22}-2C_{12})>0, \quad (C_{11}+C_{33}-2C_{13})>0 \\ &C_{11}>0, \quad C_{22}>0, \quad C_{33}>0, \quad C_{44}>0, \quad C_{55}>0, \quad C_{66}>0 \end{aligned} \qquad \textbf{(1)}$$

The elastic constants of orthorhombic SbSeI shown in Table 1 meet the Born stability criteria (mechanical stability conditions) given in equation 1. In this regard, it can be said that the SbSeI compound is mechanically stable. As known, from the elastic constants C_{11}, C_{22} and C_{33} are responsible for linear compression along the *x*-axis, *y*-axis and z-axis, respectively. If these values are large, it means the compressibility will be small. It can be said that the SbSeI compound can be compressed more along the x and z axes than the y axis. As a result of the calculations, it was seen that C_{22} among the elastic constants had the largest value. Thus, it can be said that C_{11} and C_{33} are more sensitive to pressure. Also, the value of all elastic constants increased with pressure. Again, it can be said from Table 1 that orthorhombic SbSeI is elastically anisotropic.

The elastic constant C_{44} *(*In orthorhombic structures*)* is an important parameter that governs the hardness of the material [16]. As can be seen from Table 1, this compound has small value of C_{44} indicating relatively poor shear strength. Furthermore, Bulk modulus (B) and shear module (G) are the most important parameters determining the hardness of the materials. Magnitude of the values indicates hardness of material. As known, bulk modulus is the measure of resistance against compression. The smaller size of the bulk module indicates the higher compressibility of the material, and the large size indicates the incompressibility. Usually, shear modulus is characterized as the ratio of stress to strain under shear deformation. A large shear modulus value indicates

that there is a great resistance to shear deformation, a small one indicates that this resistance is small. Bulk and shear modulus can be calculated from elastic constants with the following equations [27], [29], which are widely used in the literature.

$$B_V = \frac{1}{9}[C_{11} + C_{22} + C_{33} + 2C_{12} + 2C_{13} + 2C_{23}] \quad \textbf{(2)}$$

$$\frac{1}{B_R} = S_{11} + S_{22} + S_{33} + 2[S_{12} + S_{13} + S_{23}] \quad \textbf{(3)}$$

$$G_V = \frac{1}{15}(C_{11} + C_{22} + C_{33} - C_{12} - C_{13} - C_{23}) + \frac{1}{5}(C_{44} + C_{55} + C_{66}) \quad \textbf{(4)}$$

$$\frac{1}{G_R} = \frac{1}{15}[4(S_{11} + S_{22} + S_{33}) + 3(S_{44} + S_{55} + S_{66}) - 4(S_{12} + S_{13} + S_{23})] \quad \textbf{(5)}$$

Hill approximation is the average of Reuss (the lower limit) and Voight (the upper limit) and the result is closer to the experimental result. Mathematical expression of Hill approximation,

$$G_H = \frac{G_R + G_V}{2} \qquad B_H = \frac{B_R + B_V}{2} \quad \textbf{(6)}$$

Calculating the Young's modulus, the size of which indicates the hardness of the material, is another way of estimating the hardness of the material. Large value indicates that the material is hard. Young's modulus is (E) [27], [29],

$$E_X = \frac{9B_X G_X}{G_X + 3B_X} \quad \textbf{(7)}$$

The subscales V, R and H in the equations correspond to the Voight, Reuss and Hill approximation, respectively. X shows the V - R - H approach. Additionally, by looking at B / G ratio can be estimate ductile or brittle nature of a material. If the B / G ratio is less than 1.75, it can be classified as brittle, if it is higher than 1.75, it can be classified as ductile material [30]. The B, G and E values calculated from the elastic constants using the above equations (2-7) are given in Table 2 with available literature data. It was calculated as the B (26.15), G (12.47), B / G (2.097), and E (32.28) at ambient pressure. As can be seen in Table 2, the values obtained are consistent with the literature. By looking at the B / G ratio, it can be said that the SbSeI compound is in a ductile nature. Therefore, the SbSeI compound can be used in portable devices.

By calculating the Poisson's ratio, the nature of the bond forces can be studied. The Poisson's ratio is 0.1 for pure covalent crystals and 0.25 for pure ionic crystals [31]. The lower and upper bounds of the Poisson's ratio for central forces are 0.25 and 0.50, respectively. Poisson's ratio (ϑ) can be calculated from B and G values [32].

$$\vartheta_X = \frac{1}{2}\left[\frac{B_X - (2/3)G_X}{B_X + (1/3)G_X}\right] \quad \textbf{(8)}$$

Poisson's ratio calculated with Equation 8 were compared with the data available from the literature (Table 2). According to the Poisson's ratio given in Table 2, it can be said that ionic bonding is dominant in SbSeI compound. Also, as can be seen from the Poisson's ratio in Table 2, the SbSeI compound is under the influence of central forces. Again, while B, G and E values increased with increasing pressure, ϑ and B / G were decreased.

Table 2: Calculated elastic modules (in GPa) and Poisson's ratio**.**

P (kBar)	R	B_V	B_R	B_H	G_V	G_R	G_H	B_H/G_H	ϑ_H	E_V	E_R	E_H
0	*	26.89	25.42	26.15	13.33	11.61	12.47	2.097	0.294	34.33	30.23	32.28
0	**	26.59	25.00	25.78	13.76	12.07	12.92	2.00	0.29	-	-	33.20
4	*	29.34	28.22	28.78	14.79	13.26	14.02	2.052	0.290	37.98	34.40	36.20
8	*	32.40	31.27	31.84	16.50	15.05	15.78	2.018	0.287	42.32	38.92	40.62
12	*	35.11	34.37	34.74	18.39	16.95	17.67	1.966	0.283	46.96	43.67	45.32
16	*	37.68	37.05	37.36	20.15	18.77	19.46	1.920	0.278	51.30	48.17	49.74
40	*	51.54	51.24	51.39	28.75	27.06	27.90	1.842	0.270	72.72	69.03	70.88

* This work, ** [16]

The hardness of the material is important in terms of materials science and material engineering. So Vickers hardness was defined to express the hardness of the material. There are several models for describing Vickers hardness. Chen's model is ($k = G / B$) [33],

$$H_v = 2(k^2 G)^{0.585} - 3 \quad \textbf{(9)}$$

Experimental correlation suggested by Yousef is [34],

$$H = \frac{(1-2\vartheta)E}{6(1+\vartheta)} \quad \textbf{(10)}$$

Tian's model is [35]

$$H_v = 0{,}92\, k^{1{,}137} G^{0{,}708} \quad \textbf{(11)}$$

Table 3: Linear compressibility (TPa $^{-1}$) and hardness (GPa) of the material.

P (kBar)	β_x	β_y	β_z	Tian	Yousef	Chen
0	15.67	6.39	17.28	2.37	1.71	0.68
0 [a]	14.98	6.34	18.74	2.57	1.85	0.98
4	13.54	6.67	15.23	2.63	1.96	1.04
8	12.29	6.03	13.67	2.92	2.24	1.42
12	11.38	6.42	11.31	3.26	2.56	1.87
16	10.52	6.252	10.22	3.58	2.88	2.29
40	7.34	5.232	6.94	4.85	4.28	3.86

[a] Calculated from elastic constants reported in Reference 16.

The Vickers hardness calculated for different pressure values with different models are given in Table 3. Vickers hardness was calculated as 0.68 (Chen), 1.71 (Yousef) and 2.37 *GPa* (Tian) for SbSeI compound using the equations 9-11 given above. Li et al. (2020) stated that materials with H_v values less than 10 *GPa* can be classified as soft materials [36]. According to this result, it can be said that the SbSeI compound is not hard. Therefore, it is not expected to be used in drilling and cutting applications that require hardness. Looking at the data obtained as a result of the calculations (Table 3), it was observed that the hardness was increased corresponding to the increasing pressure value, as expected.
Linear compressibility,

$$\beta_x = S_{11} + S_{12} + S_{13} \qquad \beta_y = S_{12} + S_{22} + S_{23} \qquad \beta_z = S_{13} + S_{23} + S_{33} \quad \textbf{(12)}$$

Considering the elastic compressibility coefficients given in Table 3, calculated with Equation 12, can be said that SbSeI compound is least compressible along the y-axis.

3.2 Anisotropy of the Material

Elastic anisotropy, unusual phonon modes, dislocation dynamics, precipitation, anisotropic plastic deformation, etc. It has an important function in determining the technological use of the material, which has effects on the mechanical / physical properties of the material, such as in addition, understanding the formation of microcracks caused by anisotropy is important in terms of increasing the mechanical stability of the material. Because of this importance, anisotropy calculations are necessary[37]. Several equations are used in anisotropy calculations. These are: Universal elastic anisotropic index A^U, percent compressible anisotropy A_B, percent shear anisotropy A_G, and shear anisotropic factors A_1, A_2 and A_3, and these expressions are [27], [38], [39],

$$A_1 = \frac{4C_{44}}{C_{11}+C_{33}-2C_{13}} \quad \text{For the } \{100\} \text{ plane} \quad \textbf{(13)}$$

$$A_2 = \frac{4C_{55}}{C_{22}+C_{33}-2C_{23}} \quad \text{For the } \{010\} \text{ plane} \quad \textbf{(14)}$$

$$A_3 = \frac{4C_{66}}{C_{11}+C_{22}-2C_{12}} \quad \text{For the } \{001\} \text{ plane} \quad \textbf{(15)}$$

$$A_B = \frac{B_V - B_R}{B_V + B_R} \times 100 \qquad A_G = \frac{G_V - G_R}{G_V + G_R} \times 100 \quad \textbf{(16)}$$

$$A^U = 5\frac{G_V}{G_R} + \frac{B_V}{B_R} \geq 0 \quad \textbf{(17)}$$

If the material is elastically isotropic, the value of the A_1, A_2, A_3 are 1, otherwise it different from 1. A^U, A_B and A_G values are zero in isotropic materials. It different from zero in anisotropies. The amount of deviation from one or zero indicates the degree of anisotropy. The elastic anisotropy values calculated by Equation 13-17 are given in Table 4 together with the available literature values. According to all anisotropy expressions (From Table 4), SbSeI compound exhibits anisotropic behavior. Again, from Table 4, it is seen that {010} plane is more anisotropic than the other {100} and {001} plane.

Table 4: Anisotropy factors of the material.

P(kBar)	$A^U >= 0$	A_1	A_2	A_3	A_B	A_G
0	0.79	0.86	1.53	0.64	2.81	6.91
0 [a]	0.77	0.92	1.49	0.62	3.15	6.55
4	0.61	0.94	1.55	0.67	1.95	5.43
8	0.52	0.93	1.69	0.74	1.77	4.58
12	0.45	0.95	1.74	0.75	1.07	4.06
16	0.39	1.01	1.81	0.79	0.84	3.55
40	0.32	1.04	2.03	0.97	0.29	3.02

[a] Calculated from elastic constants reported in Reference 16.

Anisotropy was visualized in 3D and 2D with ELATE software [40] and was given in Figure 2 so that the anisotropy of the studied material can be seen more easily. In three-dimensional (two-dimensional) representation, the shape of an anisotropic material is represented by the deviation from the spherical (circle) shape. The amount of deviation from sphericity (circularity) is a measure of anisotropy. Deviations from the spherical (circle) shape are clearly visible when the 3D (2D) plots of Young, shear modulus, Poisson's ratio, and linear compressibility (Figure 2) are examined. Anisotropy is clearly visible from these 3D (2D) graphics.

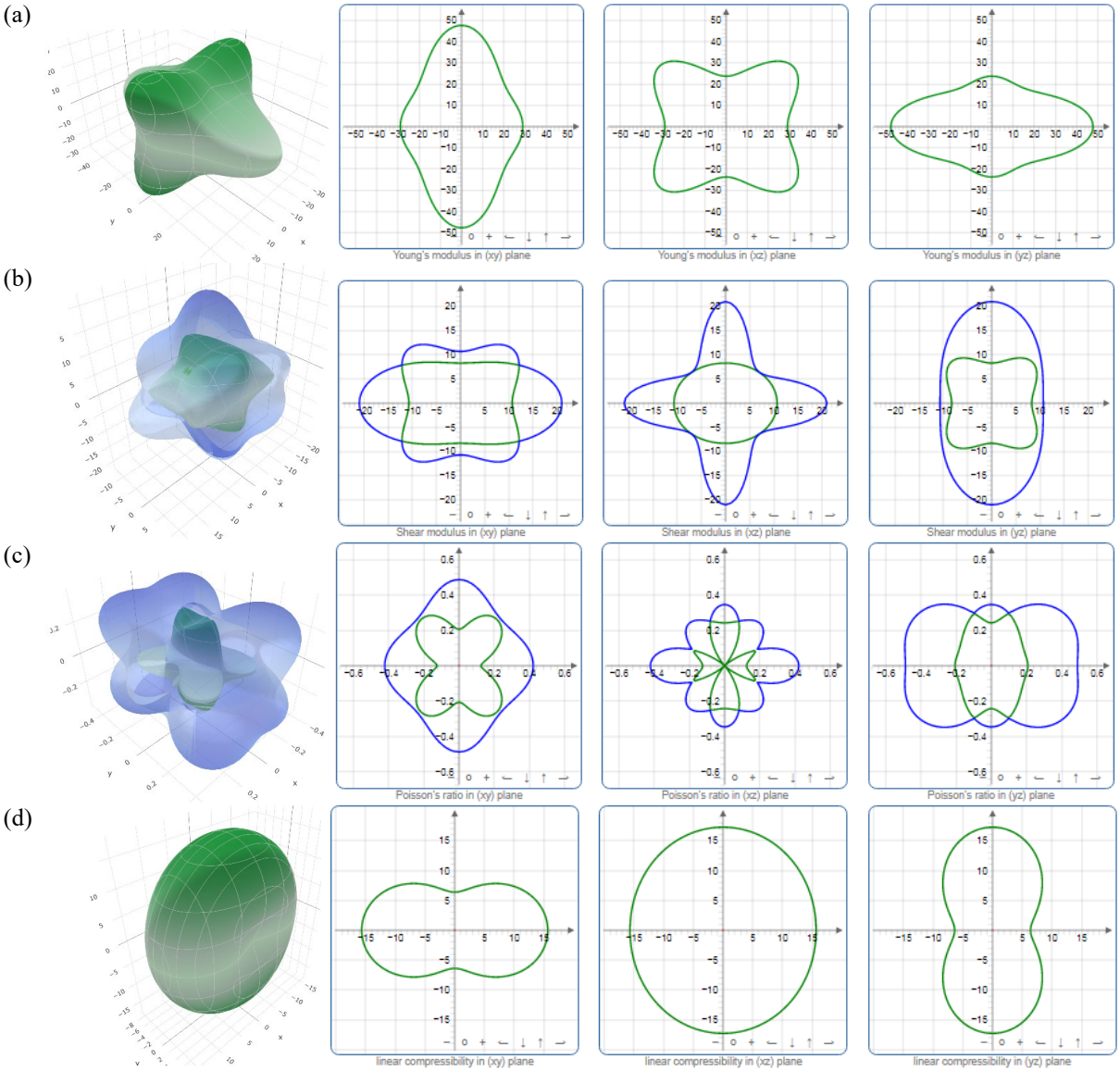

Figure 2. Two- and three-dimensional representation of Young's modulus (a), Shear modulus (b), Poisson's ratio (c), Linear compressibility (d) of SbSeI compound at ambient pressure. In the figure, the blue lines represent the maximum values, and the green lines represent the minimum values.

3.3 Thermal Properties

It is known that Debye temperature is an important basic parameter that is closely related to many physical properties such as melting temperature, cohesion energy, specific heat, thermal conductivity, thermal expansion, lattice vibration and hardness [31], [41]–[44]. Vibration warning at low temperatures is only caused by acoustic vibrations. Therefore, the Debye temperature calculated from the elastic constants at low temperatures is the same as that determined from the specific heat measurements. From the equations below, the Debye temperature can be calculated in Kelvin units [29].

$$\theta_D = \frac{h}{k_B}\left(\frac{3}{4\pi V_a}\right)^{1/3} \upsilon_m \quad (18)$$

$$\upsilon_m = \left[\left(\frac{2}{\upsilon_s^3} + \frac{1}{\upsilon_l^3}\right)/3\right]^{-1/3} \quad (19)$$

$$\upsilon_l = \sqrt{(B_x + 4G_x/3)/\rho} \qquad \upsilon_s = \sqrt{G_x/\rho} \quad (20)$$

In the equations, Planck (h), Boltzmann constant (k_B), atomic volume (V_a), average sound velocity (υ_m) in polycrystalline system. Debye temperature, υ_m, υ_l and υ_s calculated by Equation 18-20 are given in Table 5 together with the available literature values by calculating information. It is seen that the Debye temperature calculated from Table 5 is compatible with the literature value. It is seen that θ_D, υ_m, υ_l, υ_s values increase with increasing pressure value.

Table 5: Density ρ (kg / m^3), Debye temperature θ_D (K), longitudinal υ_l (m/s), transverse υ_s (m/s) and sound velocity υ_m (m/s) of the material.

P (kBar)	ρ	Voigt θ_D	Reuss θ_D	Hill			
				υ_s	υ_l	υ_m	θ_D
0	6191.7	158.1	147.8	1419.3	2628.7	1584.2	153.0
0[a]	6161.6	160.6	150.6	1446.05	2641.9	1614.5	155.6
4	6333.8	165.8	157.2	1488.0	2738.0	1660.1	161.6
8	6497.3	174.3	166.7	1558.3	2852.6	1737.8	170.6
12	6632.0	183.3	176.2	1632.2	2964.8	1819.2	179.8
16	6761.6	191.1	184.7	1696.3	3059.8	1889.6	187.9
40	7451.1	224.4	218.0	1935.2	3448.2	2153.5	221.2

[a] Calculated from elastic constants reported in Reference 16.

The Gruneisen parameter, γ_a, is an important quantity in condensed matter physics and geophysics, especially in investigating the thermodynamic behavior of materials at high pressures and temperatures [45]. The value of the Grüneisen constant range is between one and two. The acoustic Grüneisen constant defined in Eq. (21) [46]–[48] is calculated:

$$\gamma_a = \frac{3}{2}\left(\frac{3v_l^2 - 4v_s^2}{v_l^2 + 2v_s^2}\right) \quad \textbf{(21)}$$

The estimated γ_a values are given in Table 6. Since the Grüneisen constant is close to two and is inversely proportional to the thermal conductivity, its thermal conductivity is expected to be small. As can be clearly seen from Table 6, with the increase of hydrostatic pressure, the γ_a constant decreased, and the thermal conductivity increased.

The higher the Debye temperature, the stronger the chemical bonds in the crystal, while the smaller indicates the weaker the chemical bonds. Higher Debye temperature always means higher hardness [41], [42]. Higher Debye temperature corresponds to better thermal conductivity of the compound [31]. The high heat dissipation capacity of the material indicates that its thermal conductivity is high. Therefore, thermal conductivity is very important for high temperature materials [42]. The minimum thermal conductivity determines the theoretical lower limit of the intrinsic thermal conductivity of a material [49]. The minimum thermal conductivity (k_{min}) can be calculated from Equation 22-23 [31], [50].

$$k_{min} = 0.87\, k_B\, {M_a}^{-2/3}\, E^{1/2}\, \rho^{1/6} \quad \textbf{(22)}$$

$$M_a = [M/(m.N_A)] \quad \textbf{(23)}$$

The calculated M_a (mean atomic mass) and k_{min} values are given in Table 6. The minimum thermal conductivity at ambient pressure was calculated as 0.289 [50], 0.320 [51], and 0.230 $Wm^{-1}K^{-1}$ [52]. The minimum thermal conductivity of the SbSeI compound was not found in the literature. However, in terms of giving an idea to the reader, it has been compared with the results of the study of Wang et al., (2020) and Long et al., (2015). The minimum thermal conductivity of BiSeI, which is a member of the same family as SbSeI, has been reported as 0.27 $Wm^{-1}K^{-1}$ [53]. Long et al. (2015) reported that the value of k_{min} increased with increasing pressure [52]. As can be clearly seen from the data obtained with this study (Table 6), the k_{min} value of the SbSeI compound increased with increasing pressure. It can be said that this situation is compatible with the literature data. The thermal conductivities calculated for the SbSeI compound are small. The small value of the calculated minimum thermal conductivity is consistent with the Grüneisen constant.

Table 6: Calculated acoustic Grüneisen constant (γ_a), thermal conductivity (W.m^{-1}.K^{-1}).

P (kBar)	γ_a	M_a (10^{-25})	k_{min} (Clarke)	k_{min} (Cahil)	k_{min} (Long)
0	1.738	1.87	0.289	0.320	0.230
0[a]	1.685	1.81	0.293	0.339	0.245
4	1.715	1.81	0.307	0.340	0.245
8	1.697	1.81	0.326	0.361	0.261
12	1.670	1.81	0.346	0.382	0.277
16	1.645	1.81	0.364	0.401	0.291
40	1.602	1.81	0.441	0.485	0.354

[a] Calculated from elastic constants reported in Reference 16.

4. CONCLUSION

Elastic constants of SbSeI compound under 0-40 *kBar* hydro static pressure were calculated with QE and ElaStic software. It was seen that the value found in the ambient pressure was compatible with the literature data. It can be said that it is mechanically stable from the calculated elastic constants Anisotropy was calculated with different approaches and visualized with ELATE software. As a result of detailed examination of the anisotropy of the compound, it was shown that it was anisotropic. Several properties such as Vickers hardness (2.37 *GPa*), Debye temperature (153 *K*) and minimum thermal conductivity (0.289 $W.m^{-1}.K^{-1}$), which are important for materials science and engineering, were calculated. It is not a hard material as the calculated

Vickers hardness is less than 10 *GPa*. Based on this result, it can be categorized as soft material. Many physical properties of the material are closely related to the Debye temperature. Therefore, the pressure dependence of the sound velocity, the Grüneisen constant, the thermal conductivity and the Debye temperature were studied. Due to the low thermal conductivity of the SbSeI compound, it can be used as a thermal insulator in applications.

CONFLICT OF INTERESTS

The authors declare that they have no conflict of interest.

FUNDING

This study was supported by Osmaniye Korkut Ata University BAP Coordination Unit with the project numbered "OKÜBAP2018-PT2-001" named "Investigation of Structural and Mechanical Properties of SbXI (X=S, Se) Compounds Under High Pressure by Ab Initio Method".

REFERENCES

[1] B. Peng *et al.*, "Atomically sharp 1D SbSeI, SbSI and SbSBr with high stability and novel properties for microelectronic, optoelectronic, and thermoelectric applications," Mar. 2017, Accessed: Feb. 10, 2021. [Online]. Available: http://arxiv.org/abs/1703.05732

[2] Z. S. Aliev, S. S. Musaeva, D. M. Babanly, A. V. Shevelkov, and M. B. Babanly, "Phase diagram of the Sb-Se-I system and thermodynamic properties of SbSeI," ***J. Alloys Compd.***, vol. 505, no. 2, pp. 450–455, Sep. 2010, doi: 10.1016/j.jallcom.2010.06.103.

[3] W. Khan, S. Hussain, J. Minar, and S. Azam, "Electronic and Thermoelectric Properties of Ternary Chalcohalide Semiconductors: First Principles Study," ***J. Electron. Mater.***, vol. 47, no. 2, pp. 1131–1139, Feb. 2018, doi: 10.1007/s11664-017-5884-z.

[4] K. Mistewicz *et al.*, "Nanogenerator for determination of acoustic power in ultrasonic reactors," ***Ultrason. Sonochem.***, vol. 78, p. 105718, Oct. 2021, doi: 10.1016/j.ultsonch.2021.105718.

[5] A. Starczewska, "New Approach to Well-Known Compounds — Fabrication and Characterization of A V B VI C VII Nanomaterials," ***Acta Phys. Pol. A***, vol. 139, no. 4, pp. 394–400, Apr. 2021, doi: 10.12693/APhysPolA.139.394.

[6] R. Nie, M. Hu, A. M. Risqi, Z. Li, and S. Il Seok, "Efficient and Stable Antimony Selenoiodide Solar Cells," ***Adv. Sci.***, vol. 8, no. 8, Apr. 2021, doi: 10.1002/ADVS.202003172.

[7] S. K. Balakrishnan, P. C. Parambil, and E. Edri, "Mechanistic Insight into the Topotactic Transformation of Trichalcogenides to Chalcohalides," ***Chem. Mater.***, vol. 34, no. 7, pp. 3468–3478, Apr. 2022, doi: 10.1021/ACS.CHEMMATER.2C00306/SUPPL_FILE/CM2C00306_SI_001.PDF.

[8] A. Ibanez, J. C. Jumas, J. Olivier-Fourcade, E. Philippot, and M. Maurin, "Sur les chalcogeno-iodures d'antimoine SbXI(X =S, Se, Te): Structures et spectroscopie Mössbauer de121Sb," ***J. Solid State Chem.***, vol. 48, no. 2, pp. 272–283, Jul. 1983, doi: 10.1016/0022-4596(83)90082-8.

[9] A. Audzijonis, R. Sereika, and R. Žaltauskas, "Antiferroelectric phase transition in SbSI and SbSeI crystals," ***Solid State Commun.***, vol. 147, no. 3–4, pp. 88–89, Jul. 2008, doi: 10.1016/j.ssc.2008.05.008.

[10] Y. Shiozaki, E. Nakamura, and T. Mitsu, Eds., *Ferroelektrics and related substances, Inorganic substances other the oxides. Part 1 : SbSI family*. Londalt-Börnstein- Group III **condensed matte**r, 2002.

[11] G. P. Voutsas and P. J. Rentzeperis, "The crystal structure of antimony selenoiodide, SbSeI," *Zeitschrift fur Krist. -* ***New Cryst. Struct.***, vol. 161, no. 1–2, pp. 111–118, 1982, doi: 10.1524/zkri.1982.161.1-2.111.

[12] D. V. Chepur, D. M. Bercha, I. D. Turyanitsa, and V. Y. Slivka, "Peculiarities of the Energy Spectrum and Edge Absorption in the Chain Compounds $A^{V}B^{VI}C^{VII}$," ***Phys. Status Solidi***, vol. 30, no. 2, pp. 461–468, Jan. 1968, doi: 10.1002/pssb.19680300206.

[13] V. V. Sobolev, E. V. Pesterev, and V. V. Sobolev, "Absorption spectra of SbSeI and BiSeI crystals," ***Inorg. Mater.***, vol. 40, no. 1, pp. 16–19, Jan. 2004, doi: 10.1023/B:INMA.0000012172.80204.9d.

[14] K. Zickus and A. Audzijonis, "The Absorption Edge of SbSeI and BiSeI," ***Phys. Status Solidi B*****,** vol. 121, no. 1, pp. 51–53, 1984.

[15] H. Akkus, A. Kazempour, H. Akbarzadeh, and A. M. Mamedov, "Band structure and optical properties of SbSeI: density-functional calculation," ***Phys. status solidi*****,** vol. 244, no. 10, pp. 3673–3683, Oct. 2007, doi: 10.1002/pssb.200642615.

[16] T. Ozer and S. Cabuk, "First-principles study of the structural, elastic and electronic properties of SbXI (X=S, Se, Te) crystals," ***J. Mol. Model.***, vol. 24, no. 3, p. 66, Mar. 2018, doi: 10.1007/s00894-018-3608-9.

[17] T. Ozer and S. Cabuk, "Ab initio study of the lattice dynamical and thermodynamic properties of SbXI (X= S, Se, Te) compounds," ***Comput. Condens. Matter*****,** vol. 16, 2018, doi: 10.1016/j.cocom.2018.e00320.

[18] Z. Ran *et al.*, "Bismuth and antimony-based oxyhalides and chalcohalides as potential optoelectronic materials," ***npj Comput. Mater.***, vol. 4, no. 1, p. 14, Dec. 2018, doi: 10.1038/s41524-018-0071-1.

[19] J. W. Choi, B. Shin, P. Gorai, R. L. Z. Hoye, and

R. Palgrave, "Emerging Earth-Abundant Solar Absorbers," ***ACS Energy Lett.***, vol. 7, no. 4, pp. 1553–1557, Apr. 2022, doi: 10.1021/acsenergylett.2c00516.

[20] W. Everhart and J. Newkirk, "Mechanical properties of Heusler alloys," ***Heliyon***, vol. 5, no. 5, p. e01578, May 2019, doi: 10.1016/j.heliyon.2019.e01578.

[21] P. Hohenberg and W. Kohn, "Inhomogeneous electron gas," ***Phys. Rev.***, vol. 136, no. 3B, 1964, doi: 10.1103/PhysRev.136.B864.

[22] W. Kohn and L. J. Sham, "Self-consistent equations including exchange and correlation effects," ***Phys. Rev.***, vol. 140, no. 4A, 1965, doi: 10.1103/PhysRev.140.A1133.

[23] P. Giannozzi *et al.*, "QUANTUM ESPRESSO: A modular and open-source software project for quantum simulations of materials," ***J. Phys. Condens. Matter*****,** vol. 21, no. 39, 2009, doi: 10.1088/0953-8984/21/39/395502.

[24] H. J. Monkhorst and J. D. Pack, "Special points for Brillouin-zone integrations," ***Phys. Rev. B*****,** vol. 13, no. 12, pp. 5188–5192, 1976, doi: 10.1103/PHYSREVB.13.5188.

[25] R. Golesorkhtabar, P. Pavone, J. Spitaler, P. Puschnig, and C. Draxl, "ElaStic: A tool for calculating second-order elastic constants from first principles," ***Comput. Phys. Commun.***, vol. 184, no. 8, pp. 1861–1873, Aug. 2013, doi: 10.1016/j.cpc.2013.03.010.

[26] K. Momma and F. Izumi, "VESTA 3 for three-dimensional visualization of crystal, volumetric and morphology data," ***J. Appl. Crystallogr.***, vol. 44, no. 6, pp. 1272–1276, Dec. 2011, doi: 10.1107/S0021889811038970.

[27] P. Ravindran, L. Fast, P. A. Korzhavyi, B. Johansson, J. Wills, and O. Eriksson, "Density functional theory for calculation of elastic properties of orthorhombic crystals: Application to TiSi2," ***J. Appl. Phys.***, vol. 84, no. 9, pp. 4891–4904, Nov. 1998, doi: 10.1063/1.368733.

[28] O. Beckstein, J. E. Klepeis, G. L. W. Hart, and O. Pankratov, "First-principles elastic constants and electronic structure of α−Pt2 Si and PtSi," ***Phys. Rev. B***, vol. 63, no. 13, p. 134112, Mar. 2001, doi: 10.1103/PhysRevB.63.134112.

[29] D. Connétable and O. Thomas, "First-principles study of the structural, electronic, vibrational, and elastic properties of orthorhombic NiSi," ***Phys. Rev. B***, vol. 79, no. 9, p. 094101, Mar. 2009, doi: 10.1103/PhysRevB.79.094101.

[30] S. F. Pugh, "XCII. Relations between the elastic moduli and the plastic properties of polycrystalline pure metals," *London, Edinburgh,* ***Dublin Philos. Mag. J. Sci.***, vol. 45, no. 367, pp. 823–843, Aug. 1954, doi: 10.1080/14786440808520496.

[31] G. K. Arusei, M. Chepkoech, G. O. Amolo, and N. Wambua, "The elastic properties and lattice dynamics for selected 211 MAX phases: A DFT study," Nov. 2020, Accessed: Jan. 23, 2021. [Online]. Available: http://arxiv.org/abs/2011.07102

[32] U. Koroglu, S. Cabuk, and E. Deligoz, "First-principles study of structural, elastic, electronic and vibrational properties of BiCoO3," ***Solid State Sci.***, vol. 34, pp. 1–7, Aug. 2014, doi: 10.1016/j.solidstatesciences.2014.04.015.

[33] X.-Q. Chen, H. Niu, D. Li, and Y. Li, "Modeling hardness of polycrystalline materials and bulk metallic glasses," ***Intermetallics***, vol. 19, no. 9, pp. 1275–1281, Sep. 2011, doi: 10.1016/j.intermet.2011.03.026.

[34] E. S. Yousef, A. El-Adawy, and N. El-KheshKhany, "Effect of rare earth (Pr2O3, Nd2O3, Sm2O3, Eu2O3, Gd2O3 and Er2O3) on the acoustic properties of glass belonging to bismuth–borate system," ***Solid State Commun.***, vol. 139, no. 3, pp. 108–113, Jul. 2006, doi: 10.1016/J.SSC.2006.05.022.

[35] Y. Tian, B. Xu, and Z. Zhao, "Microscopic theory of hardness and design of novel superhard crystals," ***Int. J. Refract. Met. Hard Mater.***, vol. 33, pp. 93–106, Jul. 2012, doi: 10.1016/J.IJRMHM.2012.02.021.

[36] W. Liu, Y. Niu, and W. Li, "Theoretical prediction of the physical characteristic of Na3MO4 (M=Np and Pu): The first-principles calculations," ***Ceram. Int.***, vol. 46, no. 16, pp. 25359–25365, Nov. 2020, doi: 10.1016/j.ceramint.2020.07.003.

[37] G. Surucu, "Investigation of structural, electronic, anisotropic elastic, and lattice dynamical properties of MAX phases borides: An Ab-initio study on hypothetical M2AB (M = Ti, Zr, Hf; A = Al, Ga, In) compounds," ***Mater. Chem. Phys.***, vol. 203, pp. 106–117, Jan. 2018, doi: 10.1016/J.MATCHEMPHYS.2017.09.050.

[38] S. I. Ranganathan and M. Ostoja-Starzewski, "Universal Elastic Anisotropy Index," ***APS***, vol. 101, no. 5, Aug. 2008, doi: 10.1103/PhysRevLett.101.055504.

[39] D. H. Buessem and W. R. Chung, *Anisotropy in Single-Crystal Refractory Compounds*, 1st editio. Boston, MA: **Springer** US, 1968. doi: 10.1007/978-1-4899-5307-0.

[40] R. Gaillac, P. Pullumbi, and F.-X. Coudert, "ELATE: an open-source online application for analysis and visualization of elastic tensors," ***J. Phys. Condens. Matter*****,** vol. 28, no. 27, p. 275201, Jul. 2016, doi: 10.1088/0953-8984/28/27/275201.

[41] Y. Duan, Y. Wang, M. Peng, and K. Wang, "Insight into anisotropies in mechanical and thermal properties of AGdS2 (A = alkali metals) ternary gadolinium sulfides," ***Mater. Today Commun.***, vol. 26, p. 101991, Mar. 2021, doi: 10.1016/j.mtcomm.2020.101991.

[42] Y. Wang, Y. Wu, X. Wang, Y. Duan, and M.

Peng, "Insights into structural stability, electronic structure, and elastic and thermodynamic properties of A15-type Mo3X (X = Si, Ge, and Sn) compounds based on first-principles predictions," ***J. Phys. Chem. Solids***, vol. 151, p. 109925, Apr. 2021, doi: 10.1016/j.jpcs.2020.109925.

[43] W. Zuo, V. Pelenovich, D. Neena, X. Zeng, C. Liu, and D. Fu, "Determination of Debye temperatures in SmFe1-xCoxAsO superconductors by Mössbauer spectroscopy and effect of cobalt doping," ***J. Phys. Chem. Solids*****,** vol. 146, p. 109621, Nov. 2020, doi: 10.1016/j.jpcs.2020.109621.

[44] D. N. Blaschke, "Velocity dependent dislocation drag from phonon wind and crystal geometry," ***J. Phys. Chem. Solids***, vol. 124, pp. 24–35, Jan. 2019, doi: 10.1016/j.jpcs.2018.08.032.

[45] N. Korozlu, K. Colakoglu, E. Deligoz, and G. Surucu, "First-principles study of structural, elastic, lattice dynamical and thermodynamical properties of GdX (X = Bi, Sb)," ***Philos. Mag***., vol. 90, no. 14, pp. 1833–1852, May 2010, doi: 10.1080/14786430903489607.

[46] J. Kou, Y. Zhou, K.-L. Li, and L.-H. Gan, "The stability, electronic, mechanical and thermal properties of three novel superhard carbon crystals," ***Comput. Mater. Sci.***, vol. 182, p. 109758, Sep. 2020, doi: 10.1016/j.commatsci.2020.109758.

[47] C. M. I. Okoye, "Structural, elastic and electronic structure of LiCu 2 Si, LiCu 2 Ge and LiAg 2 Sn intermetallic compounds," *Comput. **Mater. Sci.***, vol. 92, pp. 141–148, Sep. 2014, doi: 10.1016/j.commatsci.2014.05.016.

[48] F. Arab, F. A. Sahraoui, K. Haddadi, A. Bouhemadou, and L. Louail, "Phase stability, mechanical and thermodynamic properties of orthorhombic and trigonal MgSiN 2 : an ab initio study," ***Phase Transitions***, vol. 89, no. 5, pp. 480–513, May 2016, doi: 10.1080/01411594.2015.1089574.

[49] G. Surucu and A. Erkisi, "The First Principles Investigation of Structural, Electronic, Mechanical and Lattice Dynamical Properties of the B and N Doped M2AX Type MAX Phases Ti2AlB0.5C0.5 and Ti2AlN0.5C0.5 Compounds," ***J. Boron*****,** Mar. 2018, doi: 10.30728/boron.333855.

[50] D. R. Clarke, "Materials selections guidelines for low thermal conductivity thermal barrier coatings," ***Surf. Coatings Technol.***, vol. 163–164, pp. 67–74, Jan. 2003, doi: 10.1016/S0257-8972(02)00593-5.

[51] D. G. Cahill, S. K. Watson, and R. O. Pohl, "Lower limit to the thermal conductivity of disordered crystals," ***Phys. Rev. B***, vol. 46, no. 10, p. 6131, Sep. 1992, doi: 10.1103/PhysRevB.46.6131.

[52] J. Long, C. Shu, L. Yang, and M. Yang, "Predicting crystal structures and physical properties of novel superhard p-BN under pressure via first-principles investigation," ***J. Alloys Compd.***, vol. 644, pp. 638–644, Sep. 2015, doi: 10.1016/J.JALLCOM.2015.04.229.

[53] D. Wang *et al.*, "Extremely low thermal conductivity from bismuth selenohalides with 1D soft crystal structure," ***Sci. China Mater.***, vol. 63, no. 9, pp. 1759–1768, Sep. 2020, doi: 10.1007/S40843-020-1407-X.